





Conversion pathways of primary defects by annealing in proton-irradiated *n*-type 4*H*-SiC

Robert Karsthof ^{*}, Marianne Etzelmüller Bathen , Augustinas Galeckas , and Lasse Vines
Centre for Materials Science and Nanotechnology, Universitetet i Oslo, Gaustadalléen 23A, N-0373 Oslo, Norway

 (Received 6 July 2020; revised 7 October 2020; accepted 3 November 2020; published 23 November 2020)

The development of defect populations after proton irradiation of *n*-type 4*H*-SiC and subsequent annealing experiments is studied by means of deep level transient (DLTS) and photoluminescence spectroscopy. A comprehensive model is suggested describing the evolution and interconversion of irradiation-induced point defects during annealing below 1000 °C. The model proposes the EH₄ and EH₅ traps frequently found by DLTS to originate from the (+/0) charge transition level belonging to different configurations of the carbon antisite-carbon vacancy (CAV) complex. Furthermore, we show that the transformation channel between the silicon vacancy (V_{Si}) and CAV is effectively blocked under *n*-type conditions, but becomes available in samples where the Fermi level has moved towards the center of the band gap due to irradiation-induced donor compensation. The annealing of V_{Si} and the carbon vacancy (V_C) is shown to be dominated by recombination with residual self-interstitials at temperatures of up to 400 °C. Going to higher temperatures, a decay of the CAV pair density is reported which is closely correlated to a renewed increase of V_C concentration. A conceivable explanation for this process is the dissociation of the CAV pair into separate carbon antisites and V_C defects. Lastly, the presented data supports the claim that the removal of free carriers in irradiated SiC is due to introduced compensating defects and not passivation of shallow nitrogen donors.

DOI: [10.1103/PhysRevB.102.184111](https://doi.org/10.1103/PhysRevB.102.184111)

I. INTRODUCTION

Silicon carbide (SiC) possesses a variety of point defects and defect complexes that are promising for quantum communication and quantum computing applications, due to both the emission of single photons upon optical excitation and the existence of high-spin states for electrons being trapped at these defect sites. Among the most studied polytypes (3*C*, 4*H*, 6*H*), 4*H*-SiC possesses the largest band gap of 3.23 eV at room temperature. It can be grown with acceptably low residual impurity concentrations such that intrinsic defects play a dominant and controllable role in material properties. Moreover, many of its intrinsic defects that can be introduced by electron or ion irradiation, or implantation, have been shown to be excellent candidates for quantum building blocks [1].

Herein, we mainly consider six intrinsic defects in 4*H*-SiC that are electrically and/or optically detectable: the carbon and silicon vacancies (V_C, V_{Si}) and self-interstitials (C_i, Si_i), the carbon antisite-carbon vacancy pair (C_{Si}V_C), and the divacancy (V_CV_{Si}). The V_C has been shown to have formation energies below 5 eV [2,3], and therefore is expected to be present in as-grown SiC, in accordance with experimental observations [4,5]. In 4*H*-SiC, V_C can occur in two crystallographically inequivalent lattice sites labeled *h* and *k* for pseudohexagonal and pseudocubic, respectively, and the formation energies of these two defects can differ by several 100 meV, depending on the charge state [2]. V_C also exhibits strong negative-*U* effects and a pronounced Jahn-Teller distortion of the singly negative charge state [6,7], leading to the direct transition from the neutral to doubly negative

(0/2−) acceptor state at around 0.7 eV below the conduction band edge *E*_C [8]. V_C seems to be an efficient center for nonradiative recombination and is therefore considered a lifetime-limiting defect [9] which has detrimental implications for bipolar devices.

The formation energy of the silicon monovacancy V_{Si} spans over a large range from around 7.5 eV under *p*-type and intrinsic conditions to as low as 4.5 eV in *n*-type SiC [2,3]. V_{Si} is mainly acceptorlike, possessing charge states between neutral and threefold negative, although a shallow donorlike (+/0) transition close to the valence band is possible [2,3]. Analogously to V_C, two configurations of V_{Si} (*h*, *k*) exist. Charge transition levels (CTLs) for the V_{Si} occur at around *E*_C − 0.7 eV for the (−/2−) and *E*_C − 0.4 eV for the (2 − /3−) levels [2,10]. V_{Si}, in contrast to V_C, does not exhibit negative-*U* character. The singly negative charge state of V_{Si} is optically addressable with a spin of *S* = 3/2 that has been shown to have a long spin coherence time [11]. This makes it an ideal candidate for both solid-state qubits as well as single-photon sources, given its favorable emission wavelengths in the near-infrared spectral range (V lines). V_{Si} defects can be controllably introduced into SiC by proton irradiation [12] and its charge state can be controlled using, e.g., Schottky barrier diodes [10].

The carbon antisite-carbon vacancy pair (CAV pair) is considered the counterpart to V_{Si} [13], because it can be formed by a single carbon hop into a neighboring V_{Si}. In *p*-type material, the formation energies of the CAV pair are significantly lower than that of the V_{Si} [2]. At around 1 eV below the conduction band edge *E*_C, the situation is reversed, with V_{Si} becoming thermodynamically slightly more favorable. Because the CAV pair involves one site from the C and another from the Si sublattice, four inequivalent configurations of the CAV pair can be realized, termed *hh*, *hk*, *kh*, and *kk*, adapting

^{*}r.m.karsthof@smn.uio.no

the notation for the monovacancies and referring to the Si site with the first and the C site with the second symbol, respectively. The CAV pair possesses three CTLs within the 4H-SiC band gap, two of which are donorlike [(2+/-) and (+/0) transitions at roughly mid-gap and 1.0–1.1 eV below E_C , respectively] and one is acceptorlike [(0/-) CTL, around 0.5 eV below E_C]. The CAV pair in its singly positive charge state is known to be an ultrabright single-photon source, emitting in the visible spectral range [14] (AB lines).

It shall be noted that the silicon antisite-vacancy pair ($\text{Si}_\text{C}\text{V}_\text{Si}$) is excluded from the list of relevant defect complexes here because it has been shown to be unstable with regard to V_C [15].

Formation of the divacancy $\text{V}_\text{Si}\text{V}_\text{C}$ (VV) [4,16] requires not only abundance of single Si and C vacancies, but also their adjacency which can be achieved at elevated temperatures via defect diffusion. Therefore, although its formation energy has been calculated to be in the same range as for V_Si and the CAV pair [17], the equilibrium concentration of VV defects depends on the extent to which the single vacancies (mostly V_Si , due to their lower migration barriers as compared to V_C [18]) are allowed to diffuse, for example, through post-annealing or during high-temperature growth or irradiation. Thermodynamic CTLs for the VV defect have been calculated in the literature to be in the range of 0.7–0.9 eV and 1.2–1.4 eV below E_C for the (-/2-) and (0/-) CTLs, respectively [19–21]. Analogously to the CAV pair, being a complex comprising two lattice sites, there are four nondegenerate configurations of the VV as well, yielding an energetic spread of each of the CTLs. The VV defect in the neutral charge state is also a known single-photon source in 4H-SiC, emitting in the infrared range around 1.2 eV [20,22].

Even though many routes have been explored on how to introduce and control certain defects by irradiation and subsequent annealing, a complete picture of the conversion pathways through which defects can be interconverted, and under which conditions this occurs, is still missing. Such a general model can be expected to be indispensable when developing post-irradiation annealing strategies to achieve a specific population of defects. This paper aims at taking a step towards such a model by studying epilayers that are proton irradiated to a wide range of fluences, and thereafter annealed in isochronal steps to increasingly higher temperatures. In each step, the defect population is monitored by means of deep level transient spectroscopy (DLTS) and photoluminescence (PL) spectroscopy in order to reveal defect interconversion and out-annealing processes.

II. EXPERIMENTAL METHODS

The investigated samples consisted of 10- μm thick, nitrogen-doped, (0001) oriented epitaxial 4H-SiC layers, purchased from Cree Inc. The doping concentration was around $N_\text{D} \approx 1 \times 10^{15} \text{ cm}^{-3}$, as determined by capacitance-voltage (C-V) measurements. The n doping of the SiC substrate amounted to about $8 \times 10^{18} \text{ cm}^{-3}$. Formation of intrinsic defects was achieved by room temperature irradiation with 1.8-MeV protons, having a projected range of 27 μm , well outside the epilayer, as simulated based on collision Monte Carlo models implemented in the SRIM package [23]. Con-

sequently, the distributions of defects generated by proton irradiation were approximately uniform throughout the top $\sim 5 \mu\text{m}$ of the epilayer, which was probed during experiment. Furthermore, diffusion of H is trap-limited in n -type 4H-SiC with diffusion on micron length scales commencing above 1300 °C [24], meaning that the implanted hydrogen is not expected to interfere with the defect conversion processes.

To suppress channeling effects, the incident beam was tilted by 8° with respect to the surface normal. Irradiation fluences were chosen between $1 \times 10^{11} \text{ cm}^{-2}$ and $6 \times 10^{13} \text{ cm}^{-2}$. This led to two subsets of samples: one in the fluence range of up to $4 \times 10^{12} \text{ cm}^{-2}$, with trap concentrations being low enough ($< 0.2N_\text{D}$) to perform DLTS measurements, and one being subjected to higher fluences that exhibited defect concentrations above the lower detectivity threshold for PL measurements. Moreover, the higher-fluence set showed full donor compensation and was therefore not suitable for DLTS initially. Note that the two sample sets (for PL and DLTS) and relatively low doping concentration ($N_\text{D} \approx 1 \times 10^{15} \text{ cm}^{-3}$) were chosen to ensure that at least one sample set contained defect concentrations in the dilute limit, and avoid monitoring nonprimary defects such as clusters and aggregates by DLTS.

After irradiation the samples were thermally annealed at 300 °C in a tube furnace in flowing N_2 ($30 \text{ cm}^3 \text{ min}^{-1}$) for 30 min to alleviate the influence of irradiation-induced unstable defects. To perform defect spectroscopy measurements, Schottky barrier diodes (SBDs) were fabricated on the epilayer surface, using electron beam-evaporated nickel patterned by deposition through a shadow mask. Before SBD fabrication, the samples underwent RCA cleaning to remove contaminations, including any SiO_2 surface layers. The SBDs were of circular cross sections and had an area of $7.85 \times 10^{-3} \text{ cm}^2$, with a Ni thickness of 150 nm. The samples intended for PL measurements were thoroughly cleaned in an ultrasonic bath in acetone and isopropyl alcohol for 5 min each, but were left untreated otherwise.

To study the influence of thermal treatment on defect conversion, isothermal annealing at increasingly higher temperatures and subsequent DLTS characterization was performed. This included the removal of SBDs before each annealing step to avoid in-diffusion and alloying of Ni into the SiC surface. For that purpose, the samples were placed in a 5:1:1 mixture of DI- H_2O : HCl : H_2O_2 at a temperature of 80 °C for 10 min, which leaves the SiC free of metal residues. After annealing, the samples were quenched to room temperature using a cold plate, and the SBDs were re-applied. The annealing steps took place at 400 °C, 600 °C, 800 °C, and 1000 °C, otherwise analogously to the conditions described for the first step above.

DLTS measurements were carried out using a high-temperature setup operating between 77 and 700 K. The measurement frequency was 1 MHz, the pulse length was 20 ms and the pulse height 10 V at a reverse bias of -10 V . Six rate windows between 20 and 640 ms were chosen for evaluation of the transients, using a standard lock-in correlation function. The concentrations of the different levels found in the measured spectra were extracted by a numerical simulation of the transients and the resulting spectra, based on assumed (variable) values for trap energy, capture cross

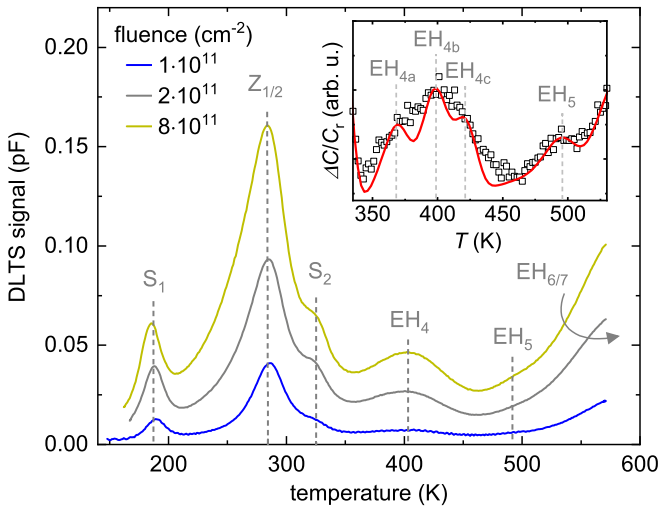


FIG. 1. DLTS spectra of 4H-SiC proton irradiated to three different fluences after an initial annealing step to 300 °C, with dominant defect levels indicated. The corresponding rate window was 1.56 s^{-1} . (Inset) High-resolution DLTS spectrum (fluence $8 \times 10^{11} \text{ cm}^{-2}$) showing the temperature region of the EH_4 and EH_5 traps, revealing three contributions to EH_4 .

section, and density of the traps [25]. The lambda correction was included for increased accuracy of the thusly determined trap concentrations. The estimated error to single-level trap concentrations determined by this method is 10^{12} cm^{-3} for the samples and measurement settings used in this study.

Photoluminescence measurements were carried out using a closed-cycle He refrigerator system (Janis, CCS450) and a 405-nm wavelength cw laser of 75 mW power as the excitation source. The focused laser beam, impinging on the sample surface at a 27° angle, yielded an excitation intensity of $\leq 1 \text{ kW cm}^{-2}$ and polarization perpendicular to the optic c axis of 4H-SiC. The PL signal was collected in a back-scattering geometry by a microscope objective (Mitutoyo, LWD 10X), spectrally filtered (long-pass LP 550-nm filter) and analyzed by an imaging spectrometer (Horiba, iHR320) coupled to an EMCCD camera (Andor, iXon Ultra 888) with a spectral resolution below 0.2 nm. A near-confocal configuration of the detection, ensured by a high numerical aperture objective and narrow slit of the imaging spectrometer, allowed for maximized collection of the PL signal from the uppermost 3–4 μm of the epilayer. Prior to the determination of PL line intensities as a qualitative measure of defect concentrations, the PL spectra were background subtracted. The estimated combined error to all line intensities by this method is 10% of the peak intensity, plus a base value that was determined from the remaining background noise which varied between wavelength windows for the different emission lines.

III. RESULTS AND DISCUSSION

A. Assessment of initial defect populations

Figure 1 shows DLTS spectra of samples irradiated to three different fluences, and subsequently annealed at 300 °C (pre-diffusion) for measurement temperatures between about 180 and 570 K, where six frequently reported trap levels

TABLE I. Properties of defect levels documented in Fig. 1 (trap energy with respect to conduction band edge, as well as assignments to specific point defects from the literature).

| Label | $E_C - E_t$ (eV) | Assignment and reference |
|-------------------|------------------|------------------------------|
| S_1 | 0.42 | V_{Si} (2–/3–) [10] |
| $Z_{1/2}$ | 0.67 | V_C (0/2–) [8,26] |
| S_2 | 0.71 | V_{Si} (1–/2–) [10] |
| EH_4 | ≈ 1.0 | |
| EH_5 | ≈ 1.1 | |
| $\text{EH}_{6/7}$ | 1.5–1.6 | V_C (2+/+/0) [8,28] |

are visible in the form of peaks or shoulders, each of them being related to one or several CTLs of a specific defect. The activation energies of these levels are summarized in Table I, together with assignments to specific point defects made in the literature. The defect levels dominating the spectra, independent of irradiation fluence, are the so-called $Z_{1/2}$ level, which has been attributed to the (0/2–) CTL of the carbon vacancy V_C [8,26], and the S center possessing the levels S_1 and S_2 , which have been identified as the (–/2–) and (2–/3–) CTLs of the silicon vacancy V_{Si} [10]. We consequently interpret their concentration as equivalent to the content of V_C and V_{Si} [27]. The feature labeled $\text{EH}_{6/7}$ at the high-temperature end of the spectra has been associated with the deeper lying (2+/+/0) CTLs of V_C in different configurations [28]. Two more peaks are noteworthy: EH_4 , a rather broad and asymmetric peak spreading between about 350 and 450 K, and EH_5 , which in the 300 °C annealed samples appears only as a weak shoulder on the low-temperature flank of $\text{EH}_{6/7}$. By using a high-resolution weighting function for the DLTS spectra, it becomes apparent that EH_4 possesses a substructure, and that three levels in total are needed to explain the considerable broadening in temperature this feature exhibits (inset of Fig. 1). The chemical identity of the defects or defect complexes producing both EH_4 and EH_5 has not been clarified so far.

While the V_C acts mainly as a nonradiative recombination center and therefore does not emit light, V_{Si} , CAV, and VV have well-documented PL lines in certain charge states. Figure 2 demonstrates the light emission from these three defects in two irradiated (to different fluences) samples at pre-diffusion conditions. Due to its energetically inequivalent configurations, the positively charged CAV pair $(C_{\text{Si}}V_C)^+$ exhibits a set of multiple emission lines in the range 648–677 nm [labeled AB lines, Fig. 2(a)] [13]. As can be seen, AB emission becomes visible for increasing irradiation fluence, and is channeled mainly into the B1/B2 line pair associated with excited states of the kk configuration of CAV [29]. Importantly, it can be stated that the CAV pair is present in our samples to detectable amounts after proton irradiation and pre-diffusion.

Figures 2(b) and 2(c) display the emission windows from the silicon vacancy. The so-called V lines appear in two regions, one of which contains the double line V1/V1' at 858.7 and 861.3 nm, and the other is the single V2 line at 916.1 nm. These have been associated with emission from excited states of the single negative V_{Si} defect on the h and

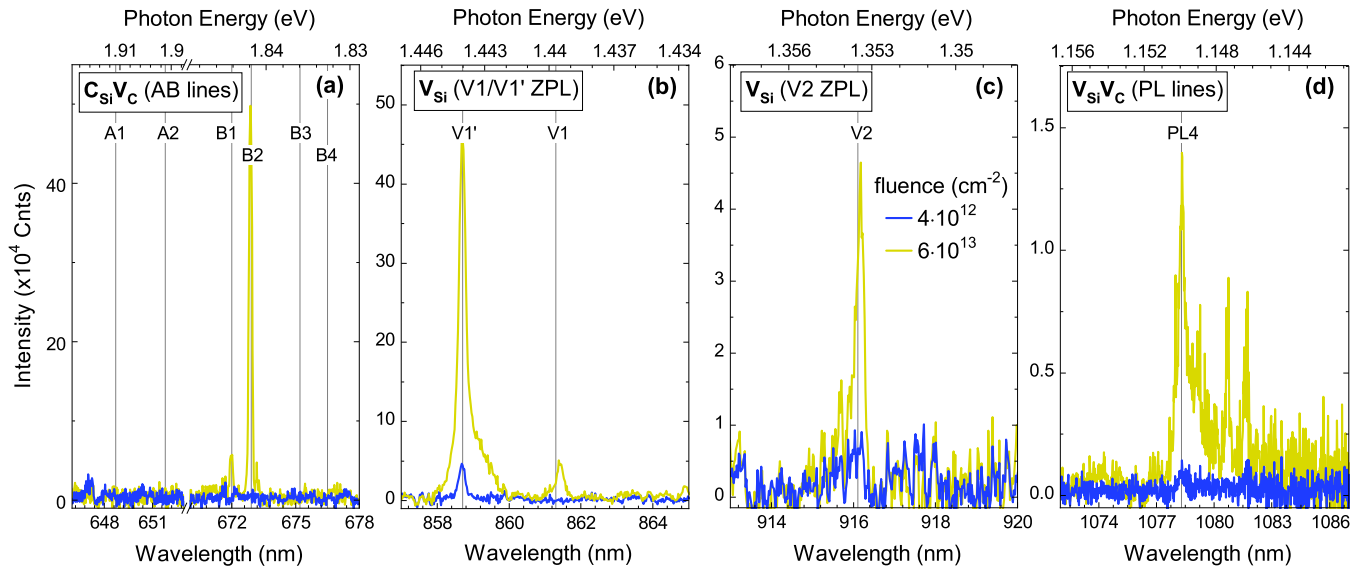


FIG. 2. PL spectra of SiC epilayers irradiated to two different fluences and post-annealed at 300 °C. Measurements were done at 10 K in four different spectral windows containing the emission of (a) the CAV defect (AB lines), V_{Si} with (b) its V1/V1' doublet and (c) V2 lines, and (d) the divacancy (PL4 line). Excitation at 405 nm, 75 mW (cw). Vertical gray lines are reference values for the emission energies. All spectra have been corrected for background.

k site for the V1/V1' and V2 lines, respectively [30]. Under the experimental conditions used here, emission from V_{Si}^- is mainly channeled into the V1' line.

Emission from the divacancy $V_{Si}V_C$, in its neutral charge state, is shown in the fourth window in Fig. 2(d). Analogously to the CAV pair, the VV is a two-component complex possessing four inequivalent configurations as well, each emitting at a specific IR wavelength in a wide range between 1077 and 1132 nm [20,31]. The lines are labeled PL1, PL2, PL3, and PL4, of which we only show the latter due to detection limitations for longer wavelengths. PL4 has been shown to belong to the hk configuration of the VV defect [20]. Similar to CAV, the divacancy is present in irradiated and pre-diffused SiC in our experiments.

B. Correlating the $C_{Si}V_C$ defect and the $EH_{4,5}$ traps

Turning to the defect identity giving rise to the EH_4 and EH_5 traps in DLTS, we start with the observation that the occurrence of these traps is correlated, i.e., either both or none of them are detectable in the same experiment. Moreover, their concentrations are always seen to be very similar, which is shown for the present study in Fig. 3. We take this as an indication for a common origin of the traps. Moreover, the $EH_{4,5}$ traps occur in concentrations similar to, but slightly lower than, those of the isolated vacancies, V_C and V_{Si} (Fig. 3). For these defects, dynamic annealing and the subsequent 300 °C anneal have been estimated to leave 3% of the vacancies initially created during proton irradiation [10]. Based on their similar concentrations, it can be stated that the rate of introduction of the defect(s) causing the $EH_{4,5}$ traps to appear is comparable, although slightly lower, than that of the monovacancies. This rules out larger defect complexes as the origin, a claim that is also supported by the fluence dependence of the $EH_{4,5}$ level concentration in Fig. 3. For a primary defect like V_{Si} and V_C , above a certain background

level, a linear relationship of concentration with fluence is expected. This is exemplified by the linear fits [32] to the monovacancy concentrations in Fig. 3. For higher-order defect complexes, the fluence dependence is expected to be superlinear, as multiple displacement events have to occur at adjacent lattice sites in order to create them. Figure 3 shows that for all four traps $EH_{4,5}$, the fluence dependence is linear, which combined with the large introduction rate narrows down the list of candidates responsible for these levels to small complexes involving V_C , V_{Si} , Si_i , and C_i , and possibly another impurity contained in the sample with significant concentrations.

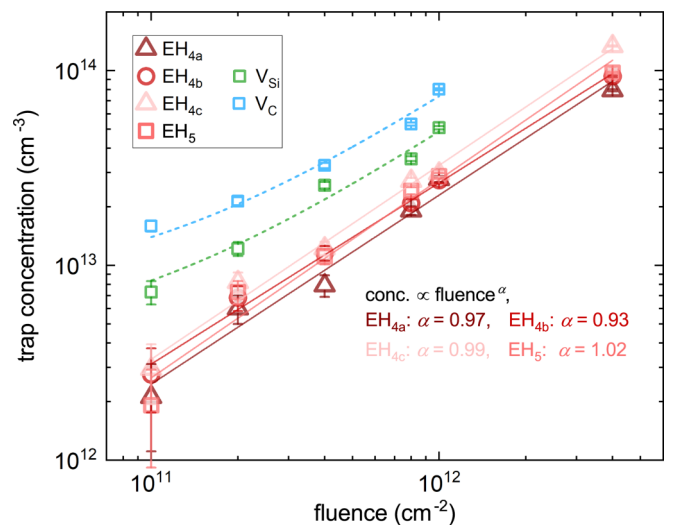


FIG. 3. Fluence dependence of the concentration of EH_4 and EH_5 traps, as well as V_C and V_{Si} , after pre-diffusion. (Compact lines) Fits demonstrating the linear fluence dependence of $EH_{4,5}$ traps. (Dashed lines) Fits to V_C and V_{Si} concentrations according to a shifted-linear model.

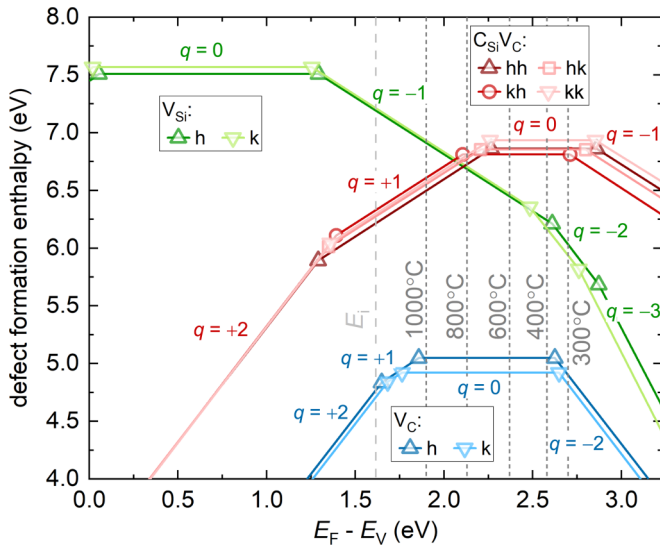


FIG. 4. Defect formation enthalpies in the carbon-rich limit for the V_{Si} , V_C , and $C_{Si}V_C$ defects in different configurations, values adapted from Ref. [2]. Position of Fermi energy for the temperatures used in our annealing experiment, and intrinsic Fermi level present after high-fluence irradiation, indicated as dashed lines.

However, a participation of interstitials is unlikely due to their low thermal stability [33] as compared to the $EH_{4,5}$ levels. This will be further supported by the thermal evolution of the defect population below. Moreover, electron irradiation experiments with energies below and above the Si displacement threshold [34,35] have shown that $EH_{4,5}$ only appear when V_{Si} is created. Therefore, the Si vacancy is likely to be involved in their formation.

Since the nitrogen content in the samples is approximately 10^{15} cm^{-3} , an additional involvement of N is conceivable, for example in the form of $N_C V_{Si}$ (NV) centers. There are, however, arguments opposing this assignment. The formation of NV centers during room-temperature irradiation is possible when a V_{Si} is formed adjacent to a N_C donor. Because this process is much less likely than the formation of V_{Si} at any lattice site, the initial density of NV centers is lower than $[V_{Si}]$ (brackets [] denote concentration) by some orders of magnitude, so we do not expect NV to be detectable in DLTS in the pre-diffusion stage—in particular not in concentrations comparable to $[V_{Si}]$ itself, which is shown in Fig. 3. Further, the $EH_{4,5}$ levels have been observed in a variety of SiC material from different sources, including nominally undoped epilayers [36]. Consequently, the candidates responsible for the $EH_{4,5}$ traps can be further narrowed down to simple and intrinsic defect complexes involving V_{Si} . This leaves mainly two possibilities: the CAV pair and the divacancy.

The formation energy diagrams for the V_C , V_{Si} , and CAV defects as calculated in Ref. [2] are reproduced in Fig. 4. CTLs related to the divacancy have not been calculated in the referenced work, but are generally expected to be in the range 0.7–0.9 eV and 1.2–1.4 eV, as discussed in the introduction. It must be stated that no prominent traps with activation energies in that range have been found by DLTS in the present work. Moreover, even though VV could be detected by PL for the highest-fluence samples in the pre-diffusion stage, $[VV]$ is

expected to be low in the lowest-fluence sample set when compared to V_{Si} , for example, while $[S_2]$ and $[EH_{4,5}]$ are of the same magnitude in these samples. We therefore argue for discarding the divacancy as the origin of the $EH_{4,5}$ traps. For the CAV pair, the formation energy diagram predicts the $(+/0)$ and the $(0/-)$ transitions to be at around 1 eV and 0.5 eV below E_C , respectively. While the latter is energetically similar to the $(-2-)$ and $(2-/3-)$ CTLs of the V_{Si} (the S_1 and S_2 centers) and the $(0/2-)$ double acceptor transition of the V_C (the $Z_{1/2}$ level), the deeper-lying $(+/0)$ CTL is energetically isolated and is therefore more suitable for the identification of the defect. An important observation of Fig. 4 is the splitting of the $(+/0)$ CTL, which we interpret as belonging to the different CAV configurations into a set of three (hk , hh , kk) at around 1.0 eV and a single one (kh) at 1.13 eV. Referring to Table I, it becomes evident that these agree well with the activation energies found for the EH_4 and EH_5 traps. As was discussed in the last section, the EH_4 peak consists of three sublevels ($EH_{4a,b,c}$) with very similar activation energies of around 1 eV, which is consistent with the hypothesis that EH_4 is produced by the hk , hh , and kk configurations of the CAV pair, while EH_5 is connected to the slightly deeper kh . Indeed, a recent EPR study [37] has found the ionization energies of the neutral CAV pair to be roughly 1.1 eV, with detectable energetic splitting between the configurations, which further supports our assignment. This provides both additional experimental confirmation of the activation energies for the CAV $(+/0)$ CTL predicted by DFT, and reaffirms the relation between the $EH_{4,5}$ levels and the CAV pair on the basis of their similar ionization levels.

We next turn to the more elusive $(0/-)$ transition at lower activation energies. It is conspicuous that $Z_{1/2}$ possesses an extended low-temperature flank towards S_1 , rendering it asymmetric in shape. This flank, upon annealing at 1000 °C, developed a clearly resolvable substructure containing four trap levels with activation energies in the range between 0.45 and 0.58 eV (indicated by arrows in Fig. 5), having signal intensities comparable to those of the $EH_{4,5}$ centers which were also present in this sample. The same substructure can be seen in DLTS spectra published by Alfieri *et al.* (Fig. 5 in Ref. [26]). These levels could therefore be the expected acceptor transitions of the CAV pair.

C. Evolution of defect concentrations with annealing

In this section, the different pathways through which intrinsic defects in n -type 4H-SiC can anneal out will be explored. The development of the defect population after each annealing step was monitored using DLTS for the low-fluence and PL for the high-fluence irradiated samples. Irradiation introduces a large variety of defects, and the dominant defects in 4H-SiC, like V_C , V_{Si} , and the complexes VV and CAV have acceptor-like states in the upper part of the band gap. Therefore it is not surprising that such experiments usually lead to the removal of free carriers with increasing irradiation fluence [38–41]. This was also observed in the present work. In Fig. 6(a) the net doping of the low-fluence samples, as determined by means of capacitance-voltage measurements, is shown after each annealing step. It can be seen that starting from a proton fluence of $4 \times 10^{11} \text{ cm}^{-2}$ an initial reduction of net doping

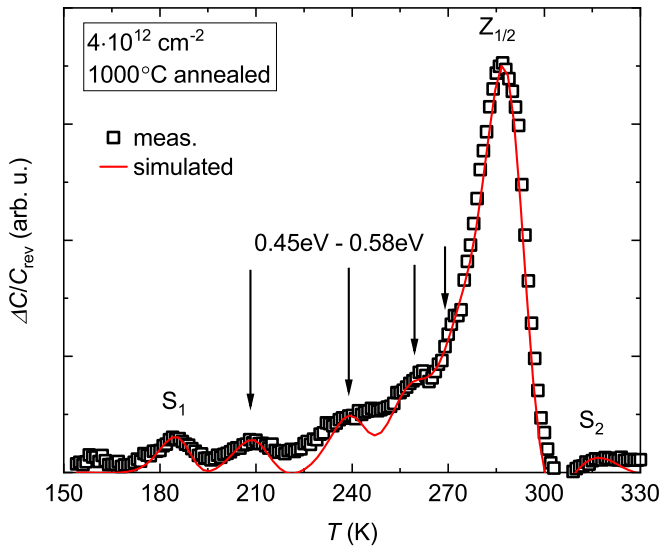


FIG. 5. High-resolution DLTS spectrum of a high-fluence irradiated and 1000 °C annealed sample, revealing a substructure of the low-temperature flank of $Z_{1/2}$ which is possibly related to the $(0/-)$ CTL of the CAV pair.

becomes noticeable. For the sample with the highest fluence in this sample set, room temperature C - V measurements were not possible in the initial state as the free carriers were entirely compensated. Interestingly, annealing can recover the free carriers almost entirely, with the temperature required to achieve recovery depending on the initial compensation. DLTS measurements on the highest-fluence sample across the full temperature range therefore became possible only after the 800 °C anneal. However, even for the partially compensated state, gradual charge carrier recovery was observed for elevated temperatures, e.g., at approximately 400 K for the initial (300 °C) stage, as is demonstrated in Fig. 6(b) where the temperature dependence of the reverse capacitance C_{rev} is shown. The temperature at which this capacitance recovery occurs decreased after each annealing step. The recovery during measurements was shown to be reversible, in contrast to the effect induced by annealing. This behavior is indicative of the compensation being due to low-stability acceptors that form independently of the doping concentration, and in contradiction to a previously suggested model according to which carrier removal is due to the irradiation-induced passivation of shallow N_C donors [38]. Introduction of compensating acceptors removes charge carriers in dependence on the Fermi level position which changes with temperature. Consequently, a partial recovery of free carriers at elevated temperatures is expected. The compensation hypothesis is also supported by the observation of the net doping density decreasing linearly with irradiation fluence, as is demonstrated by the fit (dashed line) in Fig. 6(a). Importantly, the total concentration of the detectable acceptorlike defects with known concentrations (V_C , V_{Si} , EH_4 , and EH_5) in our experiments is close to the concentration of the observed carrier removal. Hence the removal effect can, to a large extent, be explained by the aforementioned defects, indicating that there are no other prominent defects that have to be taken into account.

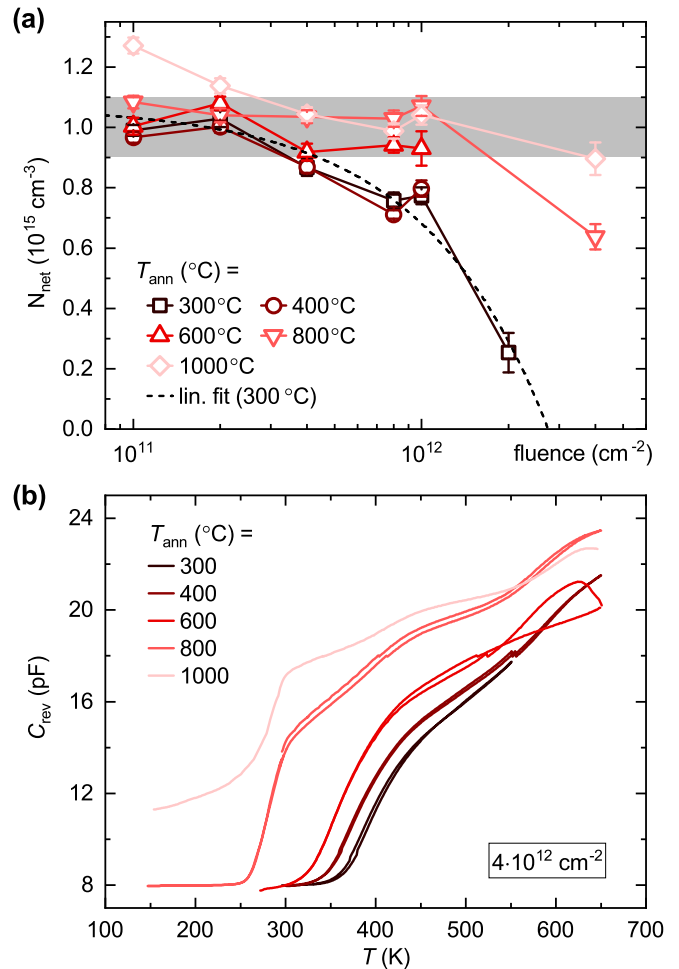


FIG. 6. (a) Net doping concentrations of low-fluence irradiated samples after annealing at different temperatures; data collected by means of C - V measurements at a reverse voltage of 10 V. (Dashed line) Linear fit to initial (300 °C) doping data. Nominal doping range highlighted in gray. (b) C_{rev} - T curves of a sample exhibiting initial compensation and partial free carrier recovery upon heating (reversible; temperature sweeps in both directions are shown) and annealing (irreversible).

1. Thermal evolution of the carbon vacancy

Figure 7 shows the development of the V_C concentration, as determined from the DLTS signal of the $Z_{1/2}$ center, with annealing at increasingly higher temperatures for the different irradiation fluences. $[V_C]$ initially drops at 400 °C and then increases with increasing annealing temperatures. The relative amount of the initial decrease is seen to be lowest for the lowest fluence, i.e., more V_C is annealed out at low temperatures when the initial defect concentration is higher. For the highest annealing temperature of 1000 °C, there is a renewed drop of $[V_C]$ for higher fluences.

A comparable observation was made by Alfieri *et al.* [26] in a multistage annealing experiment on electron-irradiated 4H-SiC. Irradiation is known to produce self-interstitials and vacancies in comparable concentrations. Dynamic annealing during the irradiation and the subsequent 300 °C pre-diffusion step are believed to lead to a significant decrease in interstitial concentration, but our results, combined with those by

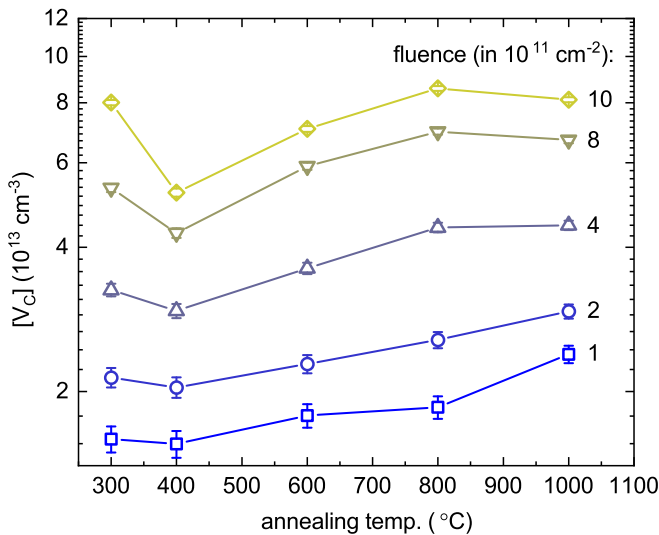


FIG. 7. C vacancy concentrations, as determined from the $Z_{1/2}$ level intensity, of SiC irradiated to various proton fluences after isochronal (30 min) annealing steps to the given temperatures.

Alferi *et al.*, demonstrate that annealing at up to 400 °C is necessary to produce a stable V_C concentration by inducing recombination with residual interstitials. In fact, based on a model for vacancy-interstitial recombination developed by Bockstedte, Mattausch, and Pankratov [33], the annihilation of these intrinsic defects is expected to occur in two stages in n -type SiC. Herein, the recombination of closely spaced vacancy-interstitial pairs happens at a comparatively low temperature of around 200 °C, whereas pairs separated by more than the nearest-neighbor distance anneal out via an interstitial diffusion-limited process that requires slightly elevated temperatures of up to 500 °C. Besides regular recombination which restores normally occupied lattice sites, formation of antisites through the same mechanism is also conceivable. However, Si_C has been shown to only possess one CTL close to the valence band [3] which is inaccessible in our experiments, such that it is not possible to distinguish antisite formation from C_i - V_C recombination. In any case, it can be stated that long-range interstitial diffusion is likely the reason for the continued annealing of V_C . The process is enhanced under n -type conditions which produce defects in more negative charge states, lowering interstitial diffusion barriers [15,33,42].

At the same time, considering the similarity of our experiments with those by Alferi *et al.*, the renewed increase of V_C concentration above 400 °C seems to be occurring irrespective of the experimental conditions and the method of irradiation. A conceivable explanation is thermal release of V_C from defect complexes. It was previously shown in Fig. 2(d) that the VV defect is actually present in the samples after the pre-diffusion step. The thermal dissociation of VV into the isolated vacancies would explain an increase of $[V_C]$. However, the VV center has been shown to be thermally stable and have a high binding energy [16,43,44], such that thermal dissociation below 1100 °C is unlikely. Another possibility of V_C release is from the CAV pair via its dissociation, which is discussed in Sec. III C 3. Analogously to VV, CAV has formed

in detectable amounts during proton irradiation, as has already been shown by PL in Fig. 2(a).

2. The silicon vacancy and the $EH_{4,5}$ centers

PL spectroscopy is a technique used for the identification and relative quantification of defect concentrations, but not their absolute values. However, because the signatures of V_{Si} in both the DLTS measurements (S center) and the PL spectra (V lines) have been identified, and the DLTS and PL results overlap for one fluence ($4 \times 10^{12} \text{ cm}^{-2}$), we normalized the PL data with regard to the DLTS concentrations in the overlapping region, and then used the established fixed multiplier to calibrate the rest of the PL data to obtain estimates for the absolute defect concentrations for both defects across the whole fluence range. This was also done for the AB lines and the $EH_{4,5}$ traps, due to the strong arguments for a shared origin between $EH_{4,5}$ and the CAV pair.

Figure 8(a) shows that there is a distinct difference between the thermal evolution of the Si vacancy at low and at high irradiation fluences, which is illustrated in the inset for a selected low- and high-fluence sample. At and below fluences of $1 \times 10^{12} \text{ cm}^{-2}$, i.e., the dilute concentration regime, the evolution is dominated by an abrupt drop of $[V_{Si}]$ for anneals at 400 °C. Upon annealing to increasingly higher temperatures, the V_{Si} concentration remains almost constant. Analogously to the V_C defect, it can be stated that the stark drop is probably due to recombination of residual Si and C interstitials that initially lack an immediate V_{Si} neighbor (Si_i - V_{Si} recombination cannot be distinguished from C_{Si} antisite formation by DLTS, as this defect does not have any CTLs in the band gap [3]). This requires somewhat elevated temperatures due to longer diffusion ranges. The migration barrier for C_i and Si_i are below 1 eV for the electrically neutral charge state and increase to around 2 eV as the Fermi level moves deeper into the band gap [42]. This means that interstitial diffusion is facilitated in the n type and partially blocked for compensated material, which is a likely explanation for the absence of a decrease in concentration in the 400 °C samples for fluences larger than 10^{12} cm^{-2} . For these compensated samples, the V_{Si} concentration evolution is instead mainly characterized by a slow decrease above 400 °C.

Figure 8(b) reveals a similar slope in the concentration/intensity development of the $EH_{4,5}$ traps and the AB lines, strengthening the relation between the CAV and $EH_{4,5}$ defects. To understand the evolution of V_{Si} , it is insightful to compare it with the simultaneous development of the CAV pair [Fig. 8(b)]. Here, a similar dichotomy of the annealing behavior can be stated. At fluences of up to $4 \times 10^{12} \text{ cm}^{-2}$, $[EH_{4,5}]$ decreases slowly with annealing temperature, by a factor of 3.75 between 300 °C and 1000 °C independent of fluence; the decrease appears to be somewhat accelerated at the highest temperatures. For the higher fluences, within the PL sample set, the 400 °C anneal induces a pronounced drop of $[CAV]$ starting from a fluence of $8 \times 10^{12} \text{ cm}^{-2}$ which is completely alleviated in the 1000 °C step. These trends with annealing temperature for the low- and high-fluence range are illustrated in the inset of Fig. 8(b) for two selected fluences.

We consider the evolution of both defect species in light of the interconversion between the V_{Si} and the CAV pair. The

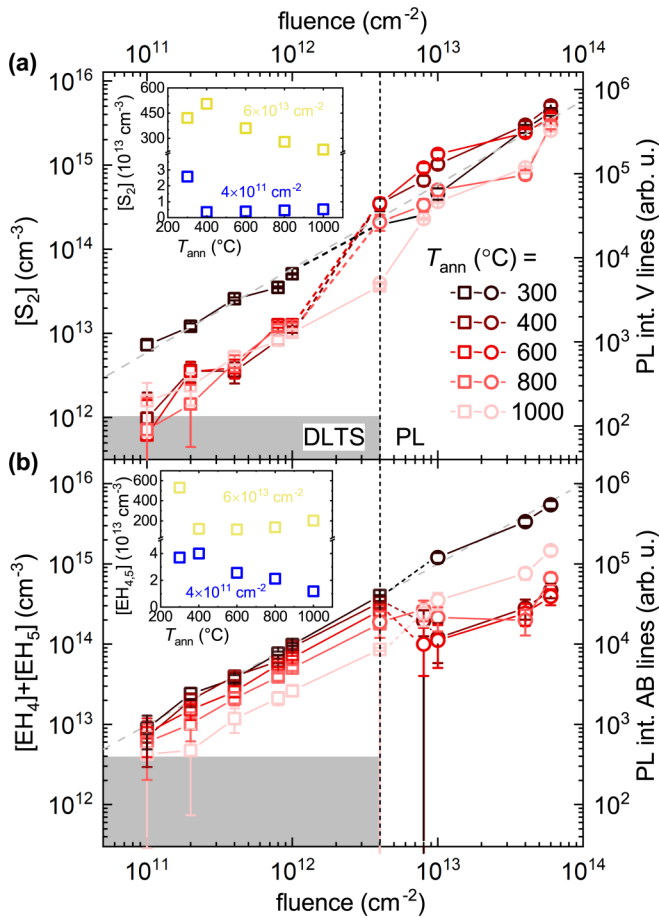


FIG. 8. Fluence dependence of the (a) S center concentration and V line intensity, and (b) of the $\text{EH}_{4,5}$ trap concentration and AB line intensity, after annealing at increasingly high temperatures. The sample irradiated to a fluence of $4 \times 10^{12} \text{ cm}^{-2}$ (dashed black line) could be characterized by both methods in several annealing stages and was therefore used for concentration calibration. Gray area marks onset of increased inaccuracy in DLTS measurement. (Gray dashed line) Linear relation with fluence. (Insets) Annealing temperature dependence of the S_2 and $\text{EH}_{4,5}$ trap concentrations for a sample from the low-fluence and high-fluence sample set.

preferential direction of this process depends on the position of the Fermi level (see formation energy diagram, Fig. 4): In p -type and intrinsic SiC, the CAV pair possesses lower formation energies than V_{Si} and will therefore be the more favorable defect species, while the situation is reversed for n -type conditions when the Fermi energy is closer to the conduction band than approximately 1 eV. Additionally, the transformation between those defects is connected to a migration barrier E_m for the C atom which also depends on the position of the Fermi level. Further, since for a fixed E_F , both V_{Si} and CAV are never in the same charge state (see Fig. 4), there are electron capture or emission processes associated with the conversion.

When V_{Si} is negatively charged (intrinsic material and high- T annealing), the conversion of V_{Si} to CAV is hindered by a migration barrier of 2.5 eV [18], but also includes double electron emission which requires an additional 1.6 eV (0.5 eV for ionization of the first and 1.1 eV for the second electron,

based on the CAV pair CTLs), consequently increasing the transformation barrier to approximately 4.1 eV. The reverse process, neutral CAV to V_{Si} , only requires free electrons available for capture, but the migration barriers are 3.5 eV and higher [18], requiring temperatures above 750 °C. However, the charge state of the CAV pair changes from neutral to 1+ just below 800 °C (see Fig. 4). The associated CAV to V_{Si} transformation barrier then increases to at least 4.2 eV [18] which shifts the required temperatures for conversion up even further. Given the fact that from 800 °C on, the CAV pair also becomes energetically more favorable than V_{Si} , we believe that the transformation of CAV to V_{Si} plays an insignificant role in n -type 4H-SiC.

Conversely, using a combined migration and emission barrier of 4.1 eV for the V_{Si} -to-CAV process, this should be observable for the highest temperatures used in this experiment. There is no such trend visible in the low-fluence samples, likely because a large fraction of V_{Si} has recombined with interstitials until 400 °C, and the remaining V_{Si} concentration is an order of magnitude lower than that of the CAV pair. If the transformation of V_{Si} to CAV occurs, its effect can be considered negligible compared to the already existing CAV defect population in the low-fluence samples. In the high-fluence (compensated) samples, however, where interstitial diffusion is suppressed, it should be observable. Indeed, the partial recovery of [CAV] for the highest temperatures may be due to this process. It is also accompanied by a decrease of $[\text{V}_{\text{Si}}]$ of comparable magnitude, as expected (see Fig. 8).

3. Correlation between $\text{EH}_{4,5}$ and $\text{Z}_{1/2}$ concentrations

What remains to be explained is the decrease of $[\text{EH}_{4,5}]$ (tentatively assigned to CAV) upon annealing, in particular the remarkable drop already at quite low temperatures for fluences of $4 \times 10^{12} \text{ cm}^{-2}$ and higher. In the low-fluence range, $[\text{EH}_{4,5}]$ decreases by a factor of 3.75 over the course of the entire annealing experiment, independent of irradiation fluence. This indicates that the mechanism behind the decrease does not include other defect species. A mechanism which would conform to this restriction is the dissociation of CAV, as was already suggested earlier when the enhanced concentration of V_{C} defects was discussed. The reaction $\text{C}_{\text{Si}}\text{V}_{\text{C}} \rightarrow \text{C}_{\text{Si}} + \text{V}_{\text{C}}$ produces an isolated carbon vacancy and a carbon on silicon-antisite C_{Si} . It requires at least a single hop of a nearest-neighbor C atom into the vacancy in order to separate the two components. C_{Si} is a defect without CTLs inside the band gap of 4H-SiC [3,45], and is therefore electrically inactive. For that reason, the dissociation of CAV pairs exclusively leads to the increase of V_{C} concentration, as it was observed in our experiments (Fig. 7).

Plotting the measured decrease of $[\text{EH}_{4,5}]$ in the low-fluence samples with annealing temperature above 400 °C versus the simultaneous increase of $[\text{Z}_{1/2}]$ from Fig. 7, it becomes apparent that these quantities agree well which each other, and share a linear 1:1 relation within experimental error (see Fig. 9). We interpret this as an indication that the decay of the concentration of CAV pairs is closely related to the gain in V_{C} density, or even the dominant contributor to this process. Since the CAV to V_{C} conversion involves a single atomic

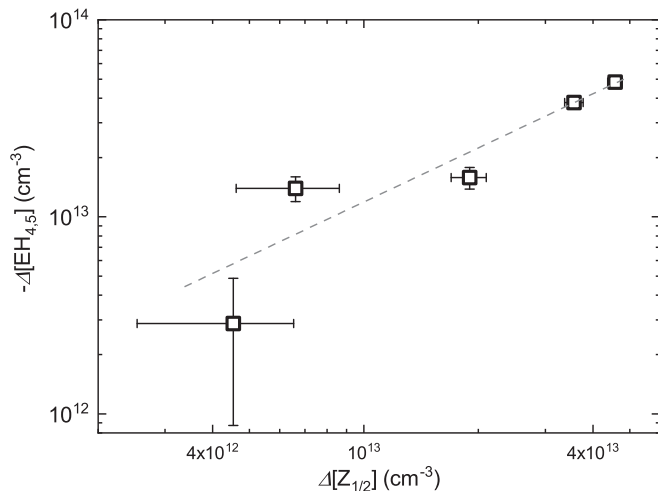


FIG. 9. Correlation of concentration differences between the $Z_{1/2}$ and $EH_{4,5}$ levels. Gray dashed line indicates a linear 1:1 relation.

hop, the corresponding hopping rate for a specific C atom at any given temperature is given by $f_{\text{hop}} = \nu_0 \exp(-E_m/k_B T)$, with E_m being the migration barrier for the C atom and ν_0 being the attempt frequency and typically on the order of a typical phonon frequency, i.e., $\nu_{\text{ph}} \approx 10^{13} \text{ s}^{-1}$. Both V_{Si} and V_{C} are tetrahedrally coordinated, therefore the concentration difference of V_{C} by conversion from CAV during an annealing experiment of duration t can be approximated by $[\Delta V_{\text{C}}] = [C_{\text{Si}}V_{\text{C}}]_0 4t\nu_{\text{ph}} \exp(-E_m/k_B T)$, where $[C_{\text{Si}}V_{\text{C}}]_0$ denotes the CAV concentration at the beginning of the experiment. We consult the data from Figs. 7 and 8(b), and taking the sample exposed to a proton fluence of $4 \times 10^{12} \text{ cm}^{-2}$ as an example, we find $[\Delta V_{\text{C}}] = 4 \times 10^{13} \text{ cm}^{-3}$ (going from 400 °C to 800 °C annealing temperatures) and $[EH_{4,5}]_0 = 3.8 \times 10^{14} \text{ cm}^{-3}$, which we suggest to identify with the CAV concentration $[C_{\text{Si}}V_{\text{C}}]_0$. Using these values, the experimentally estimated migration barrier is 3.8 eV.

However, there are not many theoretical considerations of the energetics of this process for comparison; one of the available works has been published by Wang *et al.* [17] who consider the dissociation as one possible conversion channel of the CAV pair. Based on a comparatively high dissociation barrier, which they estimate to be 5.9 eV and moreover identical to the migration barrier of V_{C} , their assessment is that this process is not of significance compared to the interconversion between CAV and V_{Si} ; however, this assessment was made assuming p -type conditions. As was already stated, shifting the Fermi level towards n -type conditions can drastically change migration barriers for defects. In fact, for the neutral C vacancy, a migration barrier between 3.7 and 4.2 eV [46] has been calculated, which is considerably lower than the value given by Wang *et al.*, and agrees well with the experimentally determined value of 3.8 eV above. Taking into account another result of Ref. [17] claiming that the dissociation energy of the CAV pair is identical for the case in which both components are second-nearest neighbors, and the case where they are located inside different unit cells, it can also be stated that a single carbon hop is probably enough to restore the electronic properties of the isolated V_{C} . Indeed,

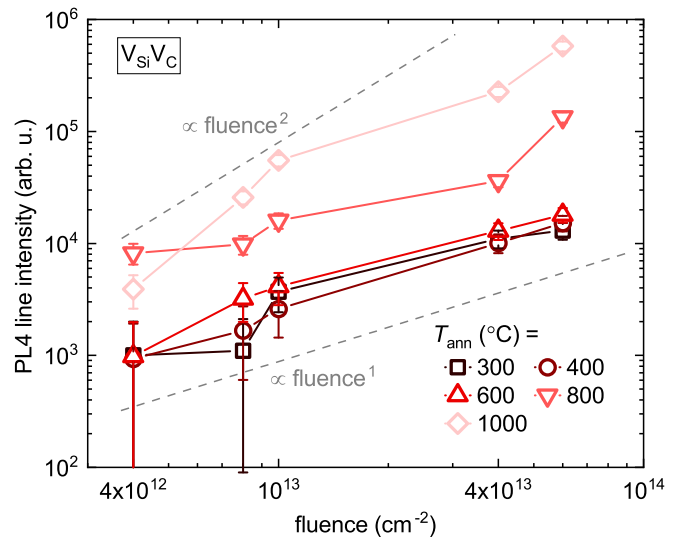


FIG. 10. Evolution of the intensity of the PL4 line (divacancy $V_{\text{Si}}V_{\text{C}}$) with annealing temperature.

Fig. 9 thus presents an additional argument for the $EH_{4,5}$ traps arising from the (+/0) CTL of the CAV pair.

As for the compensated samples, it is presently unclear if the pronounced drop in AB-line intensity can be similarly attributed to the dissociation process. If it was, there would be a fundamental difference between the compensated and the n -type samples with regard to the annealing temperature that is necessary to induce the dissociation, with a considerably lower associated barrier for lower-lying E_{F} .

4. The divacancy

The divacancy can either form during irradiation, or at elevated temperatures during post-irradiation annealing when the isolated vacancies become mobile, given a sufficiently low intersite separation compared to the defect diffusion length for the involved defects. This will be mostly due to V_{Si} diffusion, because the carbon vacancy has been shown to be immobile below 1200 °C [46]. Figure 10 displays the development of the PL4 line intensity with fluence and annealing temperature, which is taken as a qualitative measure for [VV] here. After irradiation and the 300 °C step, the divacancy is detectable in all high-fluence samples, following a linear relationship with fluence, as expected. Heating the samples to up to 600 °C only leads to a minor change of [VV]; above that temperature, the divacancy concentration exhibits a steep increase, with the highest concentrations detected after 1000 °C. [VV] now also follows an approximately quadratic relation with fluence, which can be attributed to the fact that a large portion of the defects have been formed by diffusion of V_{Si} and their pairing with V_{C} , the concentration of both of which is roughly proportional to the fluence. Son *et al.* [16] have reported on the formation of the EPR P6/7 center, which has likewise been attributed to the divacancy, in considerable amounts by annealing above 750 °C, which matches the critical VV formation temperature in this study.

The formation of VV reduces both the V_{Si} and V_{C} density to a certain extent. The resulting [VV] cannot be directly inferred from the PL measurements. However, it can be taken

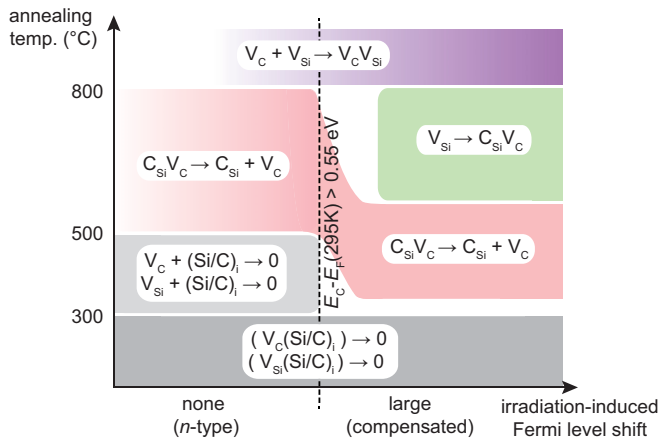


FIG. 11. Proposed model for the interconversion of defect species created in irradiated *n*-type 4H-SiC. Color gradients encode concentration of the defects produced by the reactions (darker = higher conc.).

from Fig. 7 that the trend of a slow increase of V_C density with temperature reverses at the highest annealing temperatures for irradiation fluences above $2 \times 10^{11} \text{ cm}^{-2}$. Specifically, the decrease of $[V_C]$ between 800°C and 1000°C for proton fluences of $8 \times 10^{11} \text{ cm}^{-2}$ and $1 \times 10^{12} \text{ cm}^{-2}$ amounts to $2.8 \times 10^{12} \text{ cm}^{-3}$ and $4.6 \times 10^{12} \text{ cm}^{-3}$, respectively. A decrease of similar magnitude of $[V_{Si}]$ can be inferred from Fig. 8(a) for the same two fluences. In contrast to the lower-fluence samples, here the V_C - V_C interdefect distance is already low enough such that VV can form by V_{Si} migration and binding to V_C during annealing. Therefore, the fact that the concentration change for both defects match well may be interpreted as a signature of VV formation, resulting in $[VV]$ of the order of the given changes of $[V_C]$. It should be noted, however, that these changes are in the range of the estimated error bars for trap concentrations by DLTS and therefore only confirm our model qualitatively. The low resulting $[VV]$ is also a likely explanation for why no DLTS peaks have been found in this work that can be attributed to the divacancy.

IV. DEFECT EVOLUTION MODEL

The model we propose for the annealing-induced conversion of intrinsic defects in irradiated *n*-type 4H-SiC is illustrated in Fig. 11 and will now be summarized. At annealing temperatures of 300°C and below, closely spaced pairs of Si and C vacancies and interstitials ($V_C(\text{Si/C})_i$ and $V_{Si}(\text{Si/C})_i$) annihilate easily in both *n*-type and compensated material. Increasing the temperature leads to continued recombination of non-nearest neighbor interstitial-vacancy pairs. This can only occur in *n*-type material because interstitial diffusion is severely hampered with increasingly positive charge state. The next annealing stage is the dissociation of carbon antisite-vacancy pairs via formation of individual C_{Si} and V_C defects. This process seems to be triggered more abruptly and at lower temperatures for compensated as compared to *n*-type samples. At even higher annealing temperatures, conversion of V_{Si} to CAV pair occurs in the compensated samples. This process is visible because a large

fraction of originally formed vacancies remained unannealed in the previous stage of blocked vacancy-interstitial recombination. For the highest temperatures in this experiment, the formation of divacancies via the diffusion of V_{Si} and binding to V_C defects is observed.

The relative stabilities between V_{Si} and CAV defects presented herein verify the predictions of density functional theory calculations as presented in Fig. 4, where CAV complexes are unstable with respect to dissociation in *n*-type 4H-SiC. Moreover, the findings provide important insight into the kinetics of interstitial defects, which are inferred to migrate more readily in *n*-type than intrinsic material, again validating theoretical models. Finally, we show that efficient conversion of V_{Si} to other quantum emitters, such as the divacancy and CAV pair, depends strongly on the Fermi level, representing an important advancement towards the realization of quantum devices based on point defects in 4H-SiC.

V. CONCLUSION

The defect population in proton-irradiated, *n*-type 4H-SiC epilayers and its evolution during post-annealing have been studied through a combination of optical and electrical methods. We have shown that the dominant defect species are silicon and carbon vacancies and interstitials, the carbon antisite-carbon vacancy pair (CAV), and the divacancy (VV). All these are already present after irradiation and dynamic annealing. Irradiation is also shown to lead to compensation of donors with increasing proton fluence, which can be partially reversed upon high-temperature annealing, supporting the notion of compensation by acceptor defects rather than by donor passivation.

The presented data further support the assignment of the high-temperature EH_4 and EH_5 levels observed by deep level transient spectroscopy to the $(+/-0)$ CTL of the CAV pair in its four energetically inequivalent configurations. Based on this tentative assignment, we show that a temperature-induced interconversion between the single Si vacancy (V_{Si}) and the CAV pair, as it has been reported in *p*-type material, is suppressed under *n*-type conditions. Instead, CAV defects appear to anneal out via a different route that, at the same time, leads to an equally large increase of carbon vacancy (V_C) concentration. We present a model describing this as a simple dissociation into isolated V_C and carbon antisite (C_{Si}) defects—a process which, according to our data and model, could be activated at a much lower temperature than previously expected. It also seems to occur more abruptly and at lower temperatures when the Fermi level is lower in the band gap (under compensation). We furthermore show that until 400°C , the annealing behavior of irradiated *n*-type SiC is dominated by continued recombination of vacancies V_C , V_{Si} with self-interstitials, a process which is blocked in compensated SiC. Annealing at temperatures at 800°C and above lead to the diffusion-mediated formation of divacancies $V_{Si}V_C$.

ACKNOWLEDGMENTS

The authors thank C. Zimmermann for supplying the software for simulating DLTS spectra. Financial support was kindly provided by the Research Council of Norway and the

University of Oslo through the frontier research project FUN-DAMeNT (Grant No. 251131, FriPro ToppForsk program). The Research Council of Norway is acknowledged for the

support to Project No. 274742 (NoSiCaR) and the Norwegian Micro- and Nano-Fabrication Facility, NorFab (Project No. 245963).

- [1] A. Lohrmann, B. C. Johnson, J. C. McCallum, and S. Castelletto, A review on single photon sources in silicon carbide, *Rep. Prog. Phys.* **80**, 034502 (2017).
- [2] K. Szász, V. Ivády, I. A. Abrikosov, E. Janzén, M. Bockstedte, and A. Gali, Spin and photophysics of carbon-antisite vacancy defect in 4H silicon carbide: A potential quantum bit, *Phys. Rev. B* **91**, 121201(R) (2015).
- [3] T. Kobayashi, K. Harada, Y. Kumagai, F. Oba, and Y.-I. Matsushita, Native point defects and carbon clusters in 4H-SiC: A hybrid functional study, *J. Appl. Phys.* **125**, 125701 (2019).
- [4] N. T. Son, P. Carlsson, J. ul Hassan, B. Magnusson, and E. Janzén, Defects and carrier compensation in semi-insulating 4H-SiC substrates, *Phys. Rev. B* **75**, 155204 (2007).
- [5] B. Zippelius, J. Suda, and T. Kimoto, High temperature annealing of n-type 4H-SiC: Impact on intrinsic defects and carrier lifetime, *J. Appl. Phys.* **111**, 033515 (2012).
- [6] X. T. Trinh, K. Szász, T. Hornos, K. Kawahara, J. Suda, T. Kimoto, A. Gali, E. Janzén, and N. T. Son, Negative-U carbon vacancy in 4H-SiC: Assessment of charge correction schemes and identification of the negative carbon vacancy at the quasi-cubic site, *Phys. Rev. B* **88**, 235209 (2013).
- [7] J. Coutinho, V. J. B. Torres, K. Demmouche, and S. Öberg, Theory of the carbon vacancy in 4H-SiC: Crystal field and pseudo-Jahn-Teller effects, *Phys. Rev. B* **96**, 174105 (2017).
- [8] N. T. Son, X. T. Trinh, L. S. Løvlie, B. G. Svensson, K. Kawahara, J. Suda, T. Kimoto, T. Umeda, J. Isoya, T. Makino, T. Ohshima, and E. Janzén, Negative-U System of Carbon Vacancy in 4H-SiC, *Phys. Rev. Lett.* **109**, 187603 (2012).
- [9] H. M. Ayedh, R. Nipoti, A. Hallén, and B. G. Svensson, Thermodynamic equilibration of the carbon vacancy in 4H-SiC: A lifetime limiting defect, *J. Appl. Phys.* **122**, 025701 (2017).
- [10] M. E. Bathen, A. Galeckas, J. Müting, H. M. Ayedh, U. Grossner, J. Coutinho, Y. K. Frodason, and L. Vines, Electrical charge state identification and control for the silicon vacancy in 4H-SiC, *npj Quantum Inf.* **5**, 111 (2019).
- [11] R. Nagy, M. Niethammer, M. Widmann, Y.-C. Chen, P. Udvarhelyi, C. Bonato, J. Ul Hassan, R. Karhu, I. G. Ivanov, N. T. Son, J. R. Maze, T. Ohshima, O. O. Soykal, Á. Gali, S.-Y. Lee, F. Kaiser, and J. Wrachtrup, High-fidelity spin and optical control of single silicon-vacancy centres in silicon carbide, *Nat. Commun.* **10**, 1954 (2019).
- [12] H. Kraus, D. Simin, C. Kasper, Y. Suda, S. Kawabata, W. Kada, T. Honda, Y. Hijikata, T. Ohshima, V. Dyakonov, and G. V. Astakhov, Three-dimensional proton beam writing of optically active coherent vacancy spins in silicon carbide, *Nano Lett.* **17**, 2865 (2017).
- [13] J. W. Steeds, Photoluminescence study of the carbon antisite-vacancy pair in 4H- and 6H-SiC, *Phys. Rev. B* **80**, 245202 (2009).
- [14] S. Castelletto, B. C. Johnson, V. Ivády, N. Stavrias, T. Umeda, A. Gali, and T. Ohshima, A silicon carbide room-temperature single-photon source, *Nat. Mater.* **13**, 151 (2013).
- [15] M. Bockstedte, A. Mattausch, and O. Pankratov, Ab initio study of the migration of intrinsic defects in 3C-SiC, *Phys. Rev. B* **68**, 205201 (2003).
- [16] N. T. Son, P. Carlsson, J. ul Hassan, E. Janzén, T. Umeda, J. Isoya, A. Gali, M. Bockstedte, N. Morishita, T. Ohshima, and H. Itoh, Divacancy in 4H-SiC, *Phys. Rev. Lett.* **96**, 055501 (2006).
- [17] X. Wang, M. Zhao, H. Bu, H. Zhang, X. He, and A. Wang, Formation and annealing behaviors of qubit centers in 4H-SiC from first principles, *J. Appl. Phys.* **114**, 194305 (2013).
- [18] R. Kuate Defo, X. Zhang, D. Bracher, G. Kim, E. Hu, and E. Kaxiras, Energetics and kinetics of vacancy defects in 4H-SiC, *Phys. Rev. B* **98**, 104103 (2018).
- [19] L. Gordon, A. Janotti, and C. G. Vande Walle, Defects as qubits in 3C- and 4H-SiC, *Phys. Rev. B* **92**, 045208 (2015).
- [20] B. Magnusson, N. T. Son, A. Csóré, A. Gällström, T. Ohshima, A. Gali, and I. G. Ivanov, Excitation properties of the divacancy in 4H-SiC, *Phys. Rev. B* **98**, 195202 (2018).
- [21] A. Csóré, B. Magnusson, N. T. Son, A. Gällström, T. Ohshima, I. Ivanov, and Á. Gali, First-principles study on photoluminescence quenching of divacancy in 4H-SiC, *Mater. Sci. Forum* **963**, 714 (2019).
- [22] C. P. Anderson, A. Bourassa, K. C. Miao, G. Wolfowicz, P. J. Mintun, A. L. Crook, H. Abe, J. Ul Hassan, N. T. Son, T. Ohshima, and D. D. Awschalom, Electrical and optical control of single spins integrated in scalable semiconductor devices, *Science* **366**, 1225 (2019).
- [23] J. F. Ziegler, M. Ziegler, and J. Biersack, SRIM – the stopping and range of ions in matter (2010), *Nucl. Instrum. Methods Phys. Res. Sect. B* **268**, 1818 (2010).
- [24] M. K. Linnarsson, M. S. Janson, U. Forsberg, and E. Janzén, In-diffusion, trapping and out-diffusion of deuterium in 4H-SiC substrates, *Mater. Sci. Forum* **527–529**, 637 (2006).
- [25] C. Zimmermann, Y. K. Frodason, V. Rønning, J. B. Varley, and L. Vines, Combining steady-state photo-capacitance spectra with first-principles calculations: the case of Fe and Ti in β -Ga₂O₃, *New J. Phys.* **22**, 063033 (2020).
- [26] G. Alfieri, E. V. Monakhov, B. G. Svensson, and M. K. Linnarsson, Annealing behavior between room temperature and 2000 Celsius of deep level defects in electron-irradiated n-type 4H silicon carbide, *J. Appl. Phys.* **98**, 043518 (2005).
- [27] In the former case, since two electrons are emitted because of the negative-U property of the $Z_{1/2}$ center, $[V_C] = [Z_{1/2}]/2$ is assumed.
- [28] I. D. Booker, E. Janzén, N. T. Son, J. Hassan, P. Stenberg, and E. O. Sveinbjörnsson, Donor and double-donor transitions of the carbon vacancy related EH_{6/7} deep level in 4H-SiC, *J. Appl. Phys.* **119**, 235703 (2016).
- [29] V. Ivády, I. A. Abrikosov, E. Janzén, and Á. Gali, Theoretical investigation of the single photon emitter carbon antisite-vacancy pair in 4H-SiC, *Mater. Sci. Forum* **778–780**, 495 (2014).
- [30] V. Ivády, J. Davidsson, N. T. Son, T. Ohshima, I. A. Abrikosov, and A. Gali, Identification of Si-vacancy related

- room-temperature qubits in 4H silicon carbide, *Phys. Rev. B* **96**, 161114(R) (2017).
- [31] W. F. Koehl, B. B. Buckley, F. J. Heremans, G. Calusine, and D. D. Awschalom, Room temperature coherent control of defect spin qubits in silicon carbide, *Nature (London)* **479**, 84 (2011).
- [32] Here, the simple linear model $[V_{C/Si}] = [V_{C/Si}]^0 + i_{C/Si} d$, was used where $[V_{C/Si}]^0$ are the background concentrations, $i_{C/Si}$ are the defect introduction rates by irradiation, and d is the fluence.
- [33] M. Bockstedte, A. Mattausch, and O. Pankratov, *Ab initio* study of the annealing of vacancies and interstitials in cubic SiC: Vacancy-interstitial recombination and aggregation of carbon interstitials, *Phys. Rev. B* **69**, 235202 (2004).
- [34] L. Storasta, J. P. Bergman, E. Janzén, A. Henry, and J. Lu, Deep levels created by low energy electron irradiation in 4H-SiC, *J. Appl. Phys.* **96**, 4909 (2004).
- [35] F. C. Beyer, C. G. Hemmingsson, H. Pedersen, A. Henry, J. Isoya, N. Morishita, T. Ohshima, and E. Janzén, Capacitance transient study of a bistable deep level in e^- -irradiated n-type 4H-SiC, *J. Phys. D* **45**, 455301 (2012).
- [36] C. Hemmingsson, N. T. Son, O. Kordina, J. P. Bergman, E. Janzén, J. L. Lindström, S. Savage, and N. Nordell, Deep level defects in electron-irradiated 4H-SiC epitaxial layers, *J. Appl. Phys.* **81**, 6155 (1997).
- [37] N. T. Son, P. Stenberg, V. Jokubavicius, H. Abe, T. Ohshima, J. Ul Hassan, and I. G. Ivanov, Energy levels and charge state control of the carbon antisite-vacancy defect in 4H-SiC, *Appl. Phys. Lett.* **114**, 212105 (2019).
- [38] D. Åberg, A. Hallén, P. Pellegrino, and B. G. Svensson, Nitrogen deactivation by implantation-induced defects in 4H-SiC epitaxial layers, *Appl. Phys. Lett.* **78**, 2908 (2001).
- [39] A. Castaldini, A. Cavallini, and L. Rigutti, Assessment of the intrinsic nature of deep level Z1/Z2 by compensation effects in proton-irradiated 4H-SiC, *Semicond. Sci. Technol.* **21**, 724 (2006).
- [40] V. V. Kozlovskii, V. V. Emtsev, K. V. Emtsev, N. B. Strokan, A. M. Ivanov, V. N. Lomasov, G. A. Oganessian, and A. A. Lebedev, Effect of electron irradiation on carrier removal rate in silicon and silicon carbide with 4H modification, *Semiconductors* **42**, 242 (2008).
- [41] Ž. Pastuović, R. Siegele, I. Capan, T. Brodar, S.-I. Sato, and T. Ohshima, Deep level defects in 4H-SiC introduced by ion implantation: the role of single ion regime, *J. Phys.: Condens. Matter* **29**, 475701 (2017).
- [42] X. Yan, P. Li, L. Kang, S.-H. Wei, and B. Huang, First-principles study of electronic and diffusion properties of intrinsic defects in 4H-SiC, *J. Appl. Phys.* **127**, 085702 (2020).
- [43] L. Torpo, T. E. M. Staab, and R. M. Nieminen, Divacancy in 3C- and 4H-SiC: An extremely stable defect, *Phys. Rev. B* **65**, 085202 (2002).
- [44] Q. Xu, T. Yoshiie, and M. Okada, Positron annihilation of vacancy-type defects in neutron-irradiated 4H-SiC, *J. Nucl. Mater.* **386-388**, 169 (2009).
- [45] L. Torpo, M. Marlo, T. E. M. Staab, and R. M. Nieminen, Comprehensive ab initio study of properties of monovacancies and antisites in 4H-SiC, *J. Phys.: Condens. Matter* **13**, 6203 (2001).
- [46] M. E. Bathen, J. Coutinho, H. M. Ayedh, J. Ul Hassan, I. Farkas, S. Öberg, Y. K. Frodason, B. G. Svensson, and L. Vines, Anisotropic and plane-selective migration of the carbon vacancy in SiC: Theory and experiment, *Phys. Rev. B* **100**, 014103 (2019).